Molecular Rectification of a Helical Peptide with a Redox Group in the Metal−Molecule−Metal Junction

Kazuya Kitagawa, Tomoyuki Morita, and Shunsaku Kimura*

Department of Material Chemistry, Graduate School of Engineering, Kyoto University, Kyoto-Daigaku-Katsura, Nishikyo-ku, Kyoto 615-8510, Japan

Received: February 5, 2005; In Final Form: May 30, 2005

A helical hexadecapeptide immobilized on gold via a thiophenyl group at the N-terminal was analyzed by scanning tunneling microscopy under ultrahigh vacuum to obtain the $I-V$ response at a molecular level. The attenuation factor of the electron transfer through the hexadecapeptide was determined by applying the Simons model to the $I-V$ response to show better molecular conductance of the hexadecapeptide than dodecanethiol. Chemical modification at the C-terminal of the hexadecapeptide with a ferrocene unit, on the other hand, brought about significant changes in the $I-V$ response, where the helical peptide became more conductive at the negative bias voltage. The molecular rectification behavior is due to the ferrocene unit regulating the direction of the electron transfer at the metal−molecule junction.

Introduction

Since the proposal of a molecular rectifier using a donor−spacer−acceptor (D-s-A) structure by Aviram and Ratner,[1] a large number of molecules have been examined by the test bed of the metal−molecule−metal junction to demonstrate functions such as molecular rectifiers,[2−4] wires,[5] and switches.[6] Since the development and realization of molecular electronic devices should be one stream of the ultimate goal toward miniaturization of electronic components, there is intensive interest in current−voltage ($I-V$) characteristics of single or a few molecules wired into two electrodes. The molecular rectifier is one of the most important components[7] because of its potential application for diodes and memory in molecular electronics.

In the present study, we report measurements of the $I-V$ characteristics of the helical hexadecapeptides in the metal−molecule−metal junction at a molecular level. The helical peptide is of interest as an electron transfer mediator in addition to its biological importance as well as DNA. Indeed, several groups recently reported that helical peptides act as a long-range electron-transfer mediator,[8−10] even though the mechanism of electron transfer through the peptide bridge is controvertial.[11] Helical peptides are also interesting in terms of a large dipole moment, which influences the electron transfer along the helical peptides in some cases.[8,12−14] Further, a novel hexadecapeptide (Figure 1), which has a redox group at the molecular terminal, is examined here as a molecular rectifier. When the redox group participates in the electron transfer at the metal−molecule−metal junction, asymmetric electron transfer along the helix peptide may be attained.

Recently, we have succeeded in molecular observation of the long helical peptides by scanning tunneling microscopy (STM) under ultrahigh vacuum. We extend here the molecular observation of helical peptides to the measurement of $I-V$ response at a molecular level. The electron-transfer mechanism through helical peptides and the molecular rectification of a helical peptide terminated with a redox group are discussed.

* Address correspondence to this author. E-mail: shun@scl.kyoto-u.ac.jp.

Experimental Section

Materials. All chemicals were purchased from commercial suppliers and used without further purification. AcSL16B and AcSL16Fc were synthesized by a conventional liquid-phase method and all intermediates and final products were identified by ^{1}H NMR and their purity was checked by thin-layer chromatography (TLC). The final products were further confirmed by mass spectrometry by using a JEOL JMS-HX110A spectrometer. ^{1}H NMR (400 MHz) spectra in $CDCl_3$ were measured by a Brucker AVANCE 400 spectrometer, and chemical shifts were given in δ value. TLC analyses were performed on Merck silica gel 60 F_{254} aluminum plates. Syntheses and characterizations of the precursor compound of AcSL16Fc and AcSL16B have been reported.[9,17] AcSL16Fc was synthesized from the precursor by a method similar to that used for AcSL16B.[17]

AcSL16Fc. ^{1}H NMR ($CDCl_3$, 400 MHz) δ (ppm) 0.77−1.01 (48H, m, Leu C$^{\delta}H_3$), 1.22−1.71 (75H, brm, Ala C$^{\beta}H_3$, Aib CH_3, Leu C$^{\gamma}H$ C$^{\beta}H_2$), 2.44 (3H, s, CH_3C(=O)S), 3.30−3.45 (4H, m, NHCH_2CH_2NH), 3.61−3.93 (9H, m, Ala C$^{\alpha}H$, Leu C$^{\alpha}H$), 4.23−4.86 (8H, ferrocenyl-*H*), 5.11 (2H, s, benzyl CH_2), 7.33 (5H, m, benzene), 7.49−8.25 (23H, aromatic-*H*, amide N*H*). FAB-MS (matrix; nitrobenzyl alcohol) m/z =2263 (calcd for $C_{113}H_{177}O_{22}N_{19}SFeNa$ [(M + Na)$^+$] m/z 2263.23). TLC: R_f (chloroform/methanol/acetic acid, 95/5/3, v/v/v) 0.43, R_f(chloroform/methanol, 10/1, v/v) 0.45.

Circular Dichroism (CD) Measurements. CD spectra of the peptides in an ethanol solution were measured at room temperature on a JASCO J-600 CD spectropolarimeter, using an optical cell of 0.1 cm optical path length.

SAMs Preparation. Gold substrates for reflection−absorption spectroscopy were prepared by vapor deposition of chromium (30 nm) as an adhesion layer and then gold (99.99%, 200 nm) on a slide glass. The slide glasses were cleaned ahead of deposition by concentrated H_2SO_4 followed by rigorous rinsing with distilled water and methanol. Gold substrates for STM and scanning tunneling spectroscopy (STS) were deposited

10.1021/jp050642e CCC: $30.25
Published on Web 07/01/2005

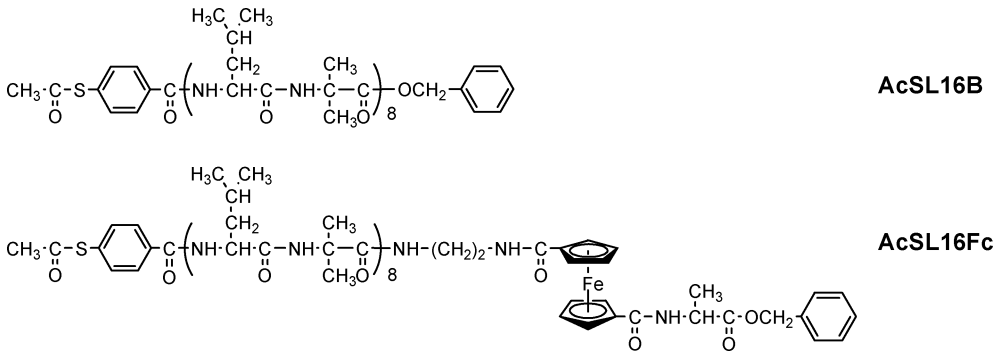

Figure 1. Molecular structures and abbreviations of the synthesized helical peptides.

on the surface of freshly cleaved mica by thermal evaporation (100 nm) and then were annealed just before preparation of the SAMs.

The helical peptides were embedded in the dodecanethiolate self-assembled monolayer (SAM) to observe a single or bundle of helical peptides. The gold substrate was incubated in an ethanol solution of dodecanethiol (1.0 mM), and then was immersed in a mixed solution of ethanol and chloroform of the peptide (0.1 mM) for 3−4 h. The peptide was treated in advance with the addition of 10 μL of ammonia water (28 wt %) per 1 mg of the peptide to deblock the acetyl group. The substrates were finally washed thoroughly with ethanol and dried in a stream of dry nitrogen gas.

Fourier Transform Infrared Reflection-Absorption Spectroscopy (FTIR-RAS). FTIR-RAS spectra were recorded on a Nicolet Magna 850 Fourier transform infrared spectrometer. For RAS measurements, a Harrick model RMA-1DG/VRA reflection attachment was used. The incident angle was set at 85°. The number of interferogram accumulations was 500. Polarization-modulation IR-RAS (PMIR-RAS) measurements were carried out on a Nicolet Magna 850 spectrometer equipped with a Hinds Instruments PEM-90 photoelastic modulator system with a II/ZS50 ZnSe head. A GWC instruments SSD-100 synchronous sampling demodulator and Nicolet SST (simultaneous synchronous technique) module and software were used for signal processing. The incident light angle was set at 80°, and the accumulation number was 1000.

The molecular orientation of the peptide monolayer on gold was determined on the basis of the amide I/amide II absorbance ratio in the FTIR RAS spectrum according to eq 1 under an assumption of a uniform distribution of the helical peptides around the surface normal:[18]

$$\frac{I_1}{I_2} = C\frac{2[^1/_2(3\cos^2\gamma - 1)][^1/_2(3\cos^2\theta_1 - 1)] + 1}{2[^1/_2(3\cos^2\gamma - 1)][^1/_2(3\cos^2\theta_2 - 1)] + 1} \quad (1)$$

where I_i, C, γ, and θ_i ($i = 1$ or 2 corresponds to amide I or amide II, respectively) represent the observed absorbance, the scaling constant ($C = 1.5$ for the peptides), the tilt angle of the helix axis from the surface normal, and the angle between the transition moment of the amide vibration mode and the helix axis, respectively. The values of the θ_1 and θ_2 were taken to be 39° and 75°, respectively.[19]

STM. STM images were acquired by UNISOKU USM-1100SA (UNISOKU Co., Ltd.) at room temperature. Measurements were performed under ultrahigh vacuum ($\sim 10^{-8}$ Pa). All images were obtained in the constant current mode and recorded at high impedances (100 GΩ or higher) to maintain the tip position over the top surface of the monolayer and to prevent the monolayer surface from any mechanical damage, which allowed direct imaging of the molecular lattice. Mechanically polished PtIr tips were used as the scanning probe. The entire STM images were unfiltered.

Current−Voltage Characteristics. $I-V$ measurements were acquired according to the following systematic procedure by using the STM. First, the peptides in the dodecanethiol SAM were scanned at a sample bias of 1.2−1.5 V and tunneling set current of 5 pA to observe the isolated helical peptides. After confirming no lateral drift of images between successive scans, scanning tunneling spectroscopy (STS) measurements were carried out at selected points. The feedback electric circuit was cut off to fix the tip−sample distance during voltage sweeps. Bias voltage was applied to the sample with taking the grounded tip as zero. STM observation was carried out in the same area after the collection of individual $I-V$ curves to check the integrity of the surface changes by STS. Those $I-V$ data, which were obtained without causing any surface changes, were used for the following analysis. The sweeps from zero to the positive bias and zero to the negative bias were separately collected. Anomalous data including no response were excluded (about 30% of the total data). All curves screened were averaged and set to zero current at zero bias to account for internal offsets generated by the microscope. The experiments were carried out on at least three different sample plates for each of SL16B and SL16Fc. Representative curves were the average of more than 160 individual curves. Nonlinear least-squares fittings for the experimental results were performed with the Igor pro software.

Calculation of Molecular Orbital Energies. The HOMO and LUMO energies of the ferrocene were estimated by ab initio calculation with the Gaussian 03 program.[20] The geometry was optimized at the Hartree−Fock (HF) level with the 6-31G(d) basis. With the optimized geometry, the single-point energy was calculated based on density functional theory with the Becke's three-parameter hybrid functional and the Lee−Yang−Parr correlation (B3LYP) method with the 6-31G(d) basis set for C and H atoms and the Dunning/Huzinaga full double-ζ (LanL2DZ) basis set for the Fe atom, affording the frontier orbital energies with respect to vacuum level. The electron affinity and ionization potential of ferrocene in the vacuum were calculated to be 0.2 and 7.2 eV, respectively, according to the reported empirical relationship of the frontier orbital energy with the ionization potential and electron affinity in the vacuum.[21] The LUMO and HOMO energies, electron affinity, and ionization potential of an amide group in a model compound (*N*-acetoamide) were calculated similarly.

Results and Discussion

Conformation in Solution and in SAMs. The peptides are composed of L-leucine and α-aminoisobutyric acid, which favor α-helical conformation. Figure 2 shows CD spectra of AcSL16B

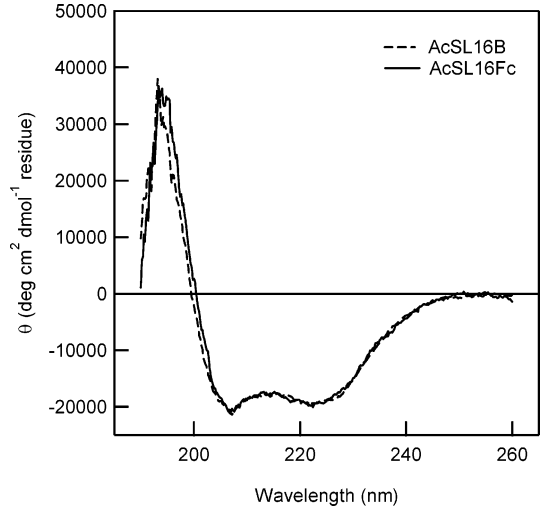

Figure 2. CD spectra of AcSL16B (dashed line) and AcSL16Fc (solid line) in ethanol at room temperature.

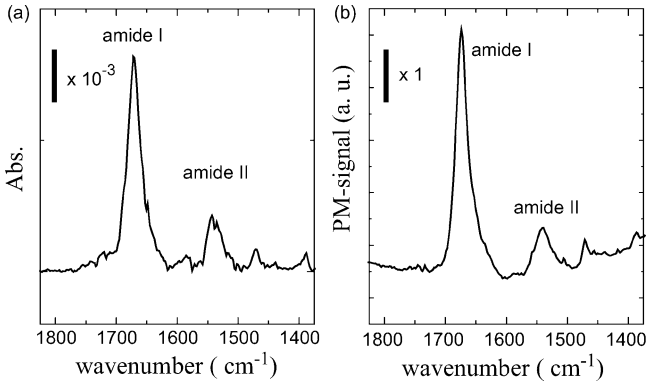

Figure 3. FTIR-RAS spectra in the amide region of (a) the SL16B SAM and (b) the SL16Fc SAM on gold. RAS spectrum for SL16Fc was recorded by PMIR-RAS.

and AcSL16Fc in ethanol solution. Both peptides showed the double minimum profile (at 208 and 222 nm), which is characteristics of the α-helical peptide.[22,23] On the basis of the mean residue ellipticity at 222 nm, the helix contents of these peptides were calculated to be 57% for both AcSL16B and AcSL16Fc.

Conformation and molecular orientation of the peptide SAMs were evaluated by FTIR-RAS measurements (Figure 3). Both peptide monolayers show the amide I and II bands around 1670 and 1542 cm^{-1}, respectively, which are consistent with the wavenumbers for α-helical peptides on the substrate previously reported.[24] The tilt angles of the helix axis from the surface normal are calculated on the basis of the absorbance intensity ratio of amide I/amide II in the RAS spectra to be 32° and 27° for SL16B and SL16Fc, respectively. These results indicate that both peptides in the SAM take α-helical conformation with nearly vertical orientation to the surface. Unfortunately, the tilt angles of the helical peptides embedded into the pre-prepared dodecanethiolate SAM could not be obtained directly from the FTIR-RAS measurements due to their weak absorbances especially in the amide II region. However, the helical peptides are considered to take vertical orientation in the mixed SAMs because the helical peptides have a cylindrical shape and are mainly inserted into defect sites of the matrix monolayer, as reported in the literature.[17] The narrow defect sites cannot accommodate the large helical peptides with horizontal orientation.

Observation of Peptide Bundles on Substrate. The peptides were embedded into the pre-prepared dodecanethiolate SAMs,[5a−c,6a−e] and the prepared mixed SAMs were subjected to STM observation in a constant-current mode under ultrahigh vacuum at room temperature. A bundle composed of a few helical peptides was observed in the mixed SAM similarly to the previous report.[17] A bundle of the SL16Fc molecules was also successfully observed in the mixed SAM (Figure 4).

In the image of the dodecanethiolate SAM (Figure 4a), the typical characteristics of the alkanethiolate SAM, such as the film domain boundaries, Au substrate terraces separated by single atom steps, and vacancy islands which are usually observed for monolayers prepared at room temperature, are identified. The inset shows the high-resolution image of the dodecanethiol SAM, which corresponds to the $(\sqrt{3} \times \sqrt{3})R30°$ hexagonal structure with a distance between the nearest neighbors of approximately 5 Å, similar to the previous report.[25]

Figure 4b shows the STM image of SL16Fc in the mixed SAM, and its magnified image is shown in Figure 4c. The bright spots are never detected in the pure dodecanethiolate SAM. SL16Fc is observed as protrusions of the helix bundle composed of several peptides, which locate at the defect sites such as structural domain boundaries, step edges between terraces, and vacancy islands of the dodecanethiolate SAM. Apparent height differences between SL16Fc and the surrounded dodecanethiolate are in the range from 2 to 9 Å depending on the number of peptide molecules in the bundles. Insertion of the helical peptides into the dodecanethiolate SAM did not adversely affect the ordering of the SAM because the crystalline structure of the dodecanethiolate SAM is clearly preserved in the mixed SAM. Although the STM tip sometimes comes in contact with the top of the exposed peptide molecules during the scanning, the peptides were visible at the same place in the following scans, indicating that the peptide molecules were firmly chemisorbed to the substrate.

Current−Voltage Characteristics. Local $I-V$ spectra were carefully collected at room temperature to study the electron transfer through the isolated peptides (Figure 5). When $I-V$ characteristics at a single molecular level are probed via metal−

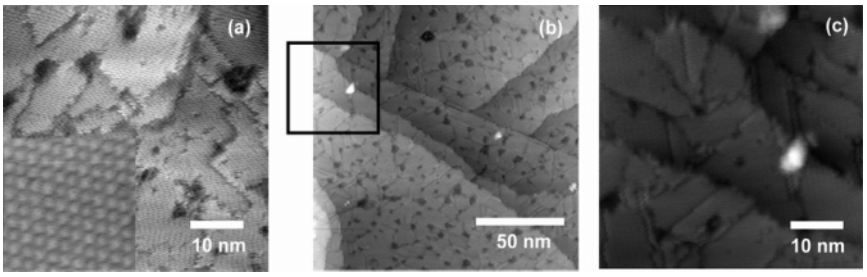

Figure 4. (a) Constant-current STM image of the dodecanethiolate SAM. (b) Constant-current STM image of SL16Fc incorporated in the dodecanethiolate SAM. Bright spots represent the isolated helix bundles of the peptide. (c) Magnified image of the isolated helix bundles of the peptide indicated by the square in panel b. These images were obtained at a sample bias of 1.2−1.5 V and a tunneling set current of 5 pA.

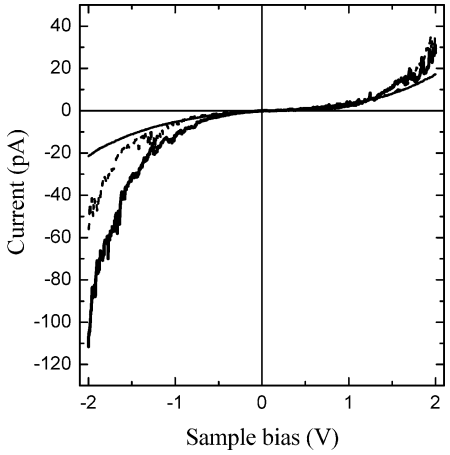

Figure 5. Averaged $I-V$ curves of dodecanethiol (thin solid line), SL16B (dashed line), and SL16Fc (thick solid line). Representative spectra were the average of more than 160 individual curves for dodecanethiol, 210 for SL16B, and 160 for SL16Fc, respectively.

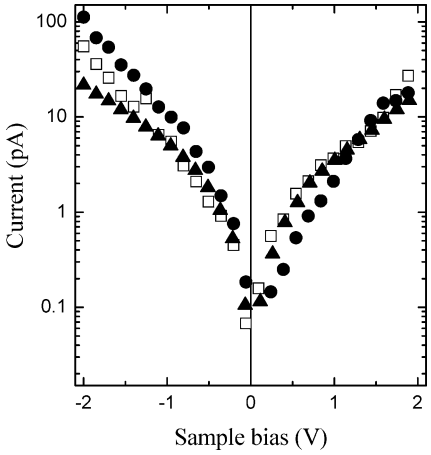

Figure 6. Semilog plot of $I-V$ curves of dodecanethiol (▲), SL16B (□), and SL16Fc (●).

molecule−metal junctions such as STM, mechanically controlled break junction, and the nanogap between electrodes prepared by electromigration, large ensembles of individual curves are prerequisite for the statistical analysis.[26,27] In our case, more than 160 individual curves, where the anomalous data were excluded, were collected and averaged.

The $I-V$ response of the dodecanethiol SAM exhibits the sigmoidal behavior (linear current response in the range of applying the low bias and exponential response at higher biases). At the low bias of 0.2 V, a current of 0.25 pA was observed, which is in agreement with the previous reports (currents between 0.1 and 0.6 pA for dodecanethiol at 0.2 V).[28−31] Slight asymmetry in the current, which is also consistent with previous reports,[29−31] is interpreted to be due to the asymmetric arrangement of the contact between molecule and electrodes. The mechanism for electron transfer through alkanethiol at the metal−molecule−metal junction is dominated by nonresonant electron tunneling.[28−31] Especially, Reed and co-workers have demonstrated the temperature independence of the electron tunneling through alkanethiol and the exponential decrease of current with the molecular length of alkanethiols.[30(a)]

In the case of SL16B, the absolute current was comparable to that of dodecanethiol within the bias of ±1.0 V. However, SL16B becomes more conductive than dodecanethiol with applying the bias beyond ±1.0 V. Asymmetric current response by SL16B in the $I-V$ curve was also observed more prominently than that of dodecanethiol. The theoretical calculation to explain the molecular conductance of the peptides will be presented in the next section together with that of dodecanethiol. A current spike was observed around −1.3 V in the $I-V$ curve even after averaging more than 160 data for SL16B (and also for SL16Fc), which might be assigned to a negative differential resistance (NDR) peak. Another group reported the NDR with *n*-alkanethiol terminated with a ferrocene unit.[32] But this feature is not discussed further at the moment because we cannot provide theoretical support for it.

$I-V$ response of SL16Fc was quite different from those of dodecanethiol and SL16B molecules. Current at the negative bias increased nearly 2-fold from that of SL16B, while the current at the positive bias was slightly suppressed from that of SL16B. These properties were clearly demonstrated in the semilog plot of $I-V$ traces as shown in Figure 6. In the case of SL16Fc, electron transfer from the gold underneath the monolayer to the STM tip occurs more favorably than that in the opposite direction. The details are discussed in the following theoretical sections.

***I*−*V* Curve Fitting with a Tunneling Model through a Rectangular Barrier.** To analyze the $I-V$ responses of the three molecules in more depth, $I-V$ curves were fitted by the Simmons model, which is the simplest model for tunneling behavior through a rectangular barrier in the metal−insulator−metal system.[33] The Simmons equation is expressed as

$$I = \frac{Ce}{4\pi^2\hbar d^2}\left\{\left(\phi - \frac{eV}{2}\right)\exp\left[-\frac{2(2m)^{1/2}}{\hbar}\alpha\left(\phi - \frac{eV}{2}\right)^{1/2}d\right] - \left(\phi + \frac{eV}{2}\right)\exp\left[-\frac{2(2m)^{1/2}}{\hbar}\alpha\left(\phi + \frac{eV}{2}\right)^{1/2}d\right]\right\} \quad (2)$$

where e is the charge of an electron, h is Planck's constant divided by 2π, d is the tunneling distance, ϕ is the barrier height, V is the applied bias, and m is the mass of an electron. C is the proportionality constant. α is a unitless adjustable parameter used in fitting.[30,31] Fittings were applied to the ±1.5 V region. By using this equation, nonlinear least-squares fitting was performed to fit eq 2 to the experimental results with three parameters, ϕ, α, and C.

At low bias, eq 2 can be approximated as

$$I = \frac{C(2m\phi)^{1/2}e^2}{h^2 d}\alpha V \exp\left[-\frac{2(2m)^{1/2}}{\hbar}\alpha(\phi)^{1/2}d\right] \quad (3)$$

The right term in this equation is not a exponential function strictly with d. Considering, however, that the exponential factor dominates in the equation,[28−30] eq 3 can be regarded as $I \approx \exp(-\beta d)$ with

$$\beta = \frac{2(2m)^{1/2}}{\hbar}\alpha(\phi)^{1/2} \quad (4)$$

where β is the structure dependent attenuation factor. Thus, β values can be calculated by using ϕ and α values obtained from the $I-V$ fitting.

Results of the curve fittings are shown in Figure 7. For the dodecanethiol and SL16B, the calculated $I-V$ curves by using eq 2 are fitted properly to the experimental data. Given the compatibility of these calculations with the experimental results, the electron tunneling through potential barriers of the molecules should be the major mechanism for the electron transfer through SL16B as well as dodecanethiol. The values of $\phi = 2.83$ and $\alpha = 0.65$ obtained here for dodecanethiol, and the β value of 1.1

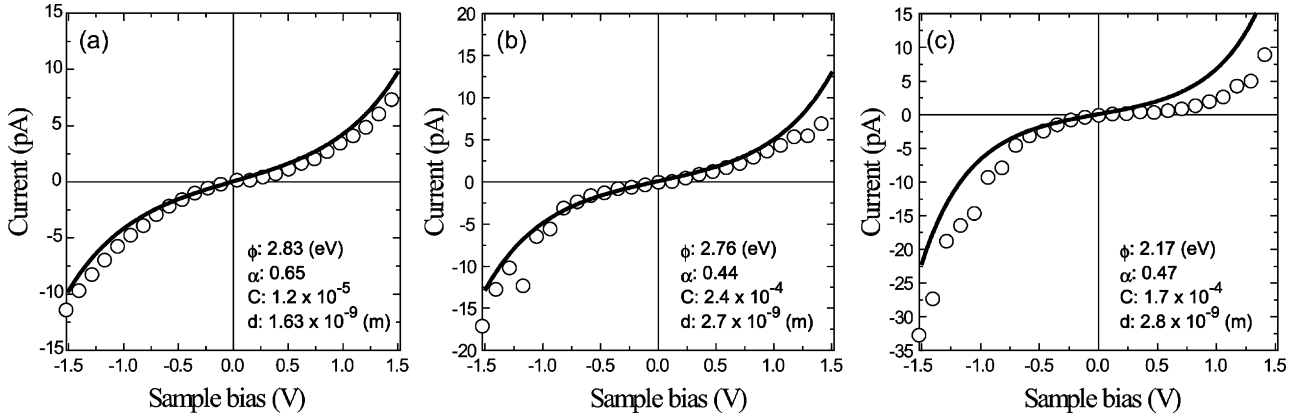

Figure 7. Curve fitting of the experimental data with the Simmons equation (eq 2). Measured data (symbols) are compared with calculations (solid lines) for (a) dodecanethiol, (b) SL16B, and (c) SL16Fc.

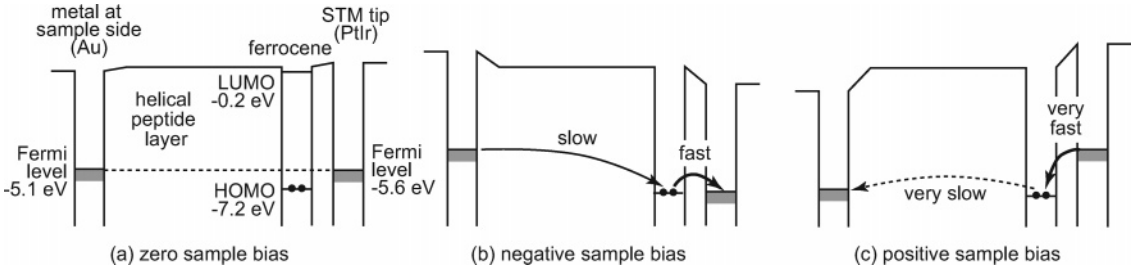

Figure 8. Energy diagrams for electron transmission in the metal-SL16Fc-STM tip junction (a) at zero sample bias, (b) at negative sample bias, and (c) at positive sample bias.

$Å^{-1}$ calculated from eq 4 are in agreement with those of previous literature.[28−31,34] The β value of 0.75 $Å^{-1}$ for SL16B from eq 4 is also agreeable with that reported for the helical peptide ($\beta = 0.66 \pm 0.1$).[35] These results clearly demonstrate that helical peptides are superior to saturated alkane chains as an electron-transfer mediator.[8,13,15a]

Fitting the $I-V$ curve of SL16Fc with eq 2 was not successful (Figure 7c), which is not surprising because the Simmons model assumes only nonresonant tunneling between two metal electrodes. As explained in the next section, electron transfer between the ferrocene moiety and the STM tip occurs in addition to normal electron tunneling at the negative sample bias. The Simmons model therefore is no longer applicable to the SL16Fc case.

Rectification Mechanisms of SL16Fc. The slightly asymmetric $I-V$ responses of dodecanethiol and SL16B without a ferrocene moiety may be accountable by the asymmetric topological arrangement of the molecule and electrodes, where one terminal of the peptides is chemically bound to gold and the other is not. However, since the rectifying behavior observed for SL16Fc carrying a ferrocene moiety is prominent, other reasons based on the ferrocene moiety should be involved in the rectification mechanism. The plausible energy diagrams for the electron transfer in the present molecular system are presented in Figure 8. The LUMO and HOMO levels of ferrocene were estimated to be −0.2 and −7.2 eV with respect to the vacuum level, respectively. Note that these levels are not mere frontier orbital energies but correspond to the ionization potential and electron affinity of ferrocene. By comparing these values with the metal Fermi level in the energy diagram, one can discuss the possibility of electron transfer between the ferrocene moiety and the metal with its driving force. We assume here that the electronic structure of the ferrocene moiety in the monolayer is close to that in the isolated form in the vacuum because the ferrocene moiety is too far from the metal to couple electronically with it. The Fermi levels of the metal underneath the monolayer (Au) and the tip (PtIr) are −5.1 and −5.6 eV, respectively.[36] It is assumed that an applied voltage evenly drops at the gold-molecule and molecule-tip interfaces according to the literature.[37,38] Figure 8a shows an energy diagram at zero sample bias, where both Fermi levels of the metals are equal. The peptide layer was taken as a simple tunneling barrier because both the HOMO level (−9.0 eV) and the LUMO level (−0.4 eV) of a peptide (amide group) are far away from the metal Fermi levels. The possibility of electron transfer via the LUMO level of the ferrocene moiety can also be ruled out because the LUMO level is far above the metal Fermi levels. On the other hand, the HOMO level is located just below the metal Fermi levels. When negative bias is applied to the metal at the sample side (gold), the Fermi level of the STM tip should be lower than the HOMO level of the ferrocene moiety (Figure 8b), which allows electron transfer from the ferrocene moiety to the adjacent tip, followed by electron donation from gold to the oxidized ferrocene moiety. This pathway in addition to normal electron tunneling should increase the apparent tunneling current. On the other hand, at positive bias, the gold Fermi level comes close to the HOMO level of ferrocene, similarly promoting electron transfer via the ferrocene moiety in the reverse direction (Figure 8c). However, the driving force at the positive bias for electron transfer through the peptide (Figure 8c) should be smaller than that at the negative bias (Figure 8b). The contribution of this electron-transfer process therefore differs depending on the bias, leading to the faster electron transfer at negative bias than that at positive bias. Considering the fact that the current through SL16Fc is comparable to that through SL16B at the positive bias, electron transfer via the ferrocene moiety at the positive bias is considered to be negligibly small. In summary, these results clearly demonstrate that the location of a redox group in the metal−molecule−metal junction has a significant influence on the overall electron flow to induce the rectification behavior.[3,4e,7]

Conclusion

The molecular conductance of dodecanethiol and two helical peptides in metal−molecule−metal junction was examined by STM. The *I*−*V* curves of the hexadecapeptide and dodecanethiol were fitted properly by the simple tunneling model. On the other hand, SL16Fc showed a prominent rectification behavior, that is, current increase was observed at the negative sample bias whereas the absolute current was comparable to that of SL16B at the positive sample bias. This result indicates that the electron transfer at the interface of the metal−molecule−metal junction can regulate the current flow through the molecule, and the placement of a proper functional group at the molecular terminal will be an important strategy for designing molecular electronic devices.

Acknowledgment. This work is partly supported by a Grant-in-Aid for Scientific Research B (15350068) from the Ministry of Education, Culture, Sports, Science, and Technology, Japan. K.K. acknowledges the Research Fellowships of the Japan Society for the Promotion of Science for Young Scientists.

References and Notes

(1) Aviram, A.; Ratner, R. M. *Chem. Phys. Lett.* **1974**, *29*, 277−283.

(2) (a) Liu, Y.; Xu, Y.; Zhu, D. *Synth. Met.* **1997**, *90*, 143−146. (b) Zhou, C.; Deshpande, M. R.; Reed, M. A.; Jones, L., II; Tour, J. M. *Appl. Phys. Lett.* **1997**, *71*, 611−613. (c) Dhirani, A.; Lin, P.-H.; Guyot-Sionnest, P.; Zehner, R. W.; Sita, L. R. *J. Chem. Phys.* **1997**, *106*, 5249−5253. (d) Kushmerick, J. G.; Holt, D. B.; Yang, J. C.; Naciri, J.; Moore, M. H.; Shashidhar, R. *Phys. Rev. Lett.* **2002**, *89*, 086802-1−086802-4.

(3) (a) Krzeminski, C.; Delerue, C.; Allan, G.; Vuillaume, D.; Metzger, R. M. *Phys. Rev.* **2001**, *B64*, 085405. (b) Chabinyc, M. L.; Chen, X.; Holmlin, R. E.; Jacobs, H.; Skulason, H.; Frisbie, C. D.; Mujica, V.; Ratner, M. A.; Rampi, M. A.; Whitesides, G. M. *J. Am. Chem. Soc.* **2002**, *124*, 11731.

(4) (a) Metzger, R. M.; Chen, B.; Hopfner, U.; Lakshmikantham, M. V.; Vuillaume, D.; Kawai, T.; Wu, X. L.; Tachibana, H.; Hughes, T. V.; Sakurai, H.; Baldwin, J. W.; Hosch, C.; Cava, M. P.; Brehmer, L.; Ashwell, G. J. *J. Am. Chem. Soc.* **1997**, *119*, 10455−10466. (b) Metzger, R. M. *Acc. Chem. Res.* **1999**, *32*, 950−957. (c) Xu, T.; Peterson, I. R.; Lakshmikantham, M. V.; Metzger, R. M. *Angew. Chem., Int. Ed.* **2001**, *40*, 1749−1752. (d) Ng, M.-K.; Lee, D.-C.; Yu, L. *J. Am. Chem. Soc.* **2002**, *124*, 11862−11863. (e) Ashwell, G. J.; Tyrrell, W. D.; Whittam, A. J. *J. Am. Chem. Soc.* **2004**, *126*, 7102−7110.

(5) (a) Bumm, L. A.; Arnold, J. J.; Cygan, M. T.; Dunbar, T. D.; Burgin, T. P.; Jones, L., II; Allara, D. L.; Tour, J. M.; Weiss, P. S. *Science* **1996**, *271*, 1705−1707. (b) Cygan, M. T.; Dunbar, T. D.; Arnold, J. J.; Bumm, L. A.; Shedlock, N. F.; Burgin, T. P.; Jones, L., II; Allara, D. L.; Tour, J. M.; Weiss, P. S. *J. Am. Chem. Soc.* **1998**, *120*, 2721−2732. (c) Reed, M. A.; Zhou, C.; Muller, C. J.; Burgin, T. P.; Tour, J. M. *Science* **1997**, *278*, 252−254.

(6) (a) Donhauser, Z. J.; Mantooth, B. A.; Kelly, K. F.; Bumm, L. A.; Monnell, J. D.; Stapleton, J. J.; Price, D. W., Jr.; Rawlett, A. M.; Allara, D. L.; Tour, J. M.; Weiss, P. S. *Science* **2001**, *292*, 2303−2307. (b) Donhauser, Z. J.; Mantooth, B. A.; Pearl, T. P.; Kelly, K. F.; Nanayakkara, S. U.; Weiss, P. S. *Jpn. J. Appl. Phys.* **2002**, *41*, 4871−4877. (c) Lewis, P. A.; Inman, C. E.; Yao, Y.; Tour, J. M.; Hutchison, J. E.; Weiss, P. S. *J. Am. Chem. Soc.* **2004**, *126*, 12214−12215. (d) Ramachandran, G. K.; Hopson, T. J.; Rawlett, A. M.; Nagahara, L. A.; Primak, A.; Lindsay, S. M. *Science* **2003**, *300*, 1413−1416. (e) Wassel, R. A.; Fuierer, R. R.; Kim, N.; Gorman, C. B. *Nano Lett.* **2003**, *3*, 1617−1620. (f) Chen, J.; Reed, M. A.; Raelett, A. M.; Tour, J. M. *Science* **1999**, *286*, 1550−1552. (g) Collier, C. P.; Mattersteig, G.; Wong, E. W.; Luo, Y.; Beverly, K.; Sampaio, J.; Raymo, F. M.; Stoddart, J. F.; Heath, J. R. *Science* **2000**, *289*, 1172−1175.

(7) Metzger, R. M. *Chem. Rev.* **2003**, *103*, 3803−3834.

(8) Morita, T.; Kimura, S. *J. Am. Chem. Soc.* **2003**, *125*, 8732−8733.

(9) Sek, S.; Sepiol, A.; Tolak, A.; Misicka, A.; Bilewicz, R. *J. Phys. Chem. B* **2004**, *108*, 8102−8105.

(10) Malak, R. A.; Gao, Z.; Wishart, J. F.; Isied, S. S. *J. Am. Chem. Soc.* **2004**, *126*, 13888−13889.

(11) (a) Isied, S. S.; Ogawa, M. Y.; Wishart, J. F. *Chem. Rev.* **1992**, *92*, 381−394. (b) Wuttke, D. S.; Bjerrum, M. J.; Winkler, J. R.; Gray, H. B. *Science* **1992**, *256*, 1007−1009. (c) Petrov, E. G.; Shevchenko, Y. V.; Teslenko, V. I. *J. Chem. Phys.* **2001**, *115*, 7107−7122. (d) Zheng, Y.; Case, M. A.; Wishart, J. F.; McLendon, G. L. *J. Phys. Chem. B* **2003**, *107*, 7288−7292 (e) Kraatz, H.-B.; Bediako-Amoa, I.; Gyepi-Garbrah, S. H.; Sutherland, T. C. *J. Phys. Chem. B* **2004**, *108*, 20164−20172. (f) Polo, F.; Antonello, S.; Formaggio, F.; Toniolo, C.; Maran, F. *J. Am. Chem. Soc.* **2005**, *127*, 492−493.

(12) (a) Galoppini, E.; Fox, M. A. *J. Am. Chem. Soc.* **1996**, *118*, 2299−2300. (b) Fox, M. A.; Galoppini, E. *J. Am. Chem. Soc.* **1997**, *119*, 5277−5285.

(13) Morita, T.; Kimura, S.; Kobayashi, S.; Imanishi, Y. *J. Am. Chem. Soc.* **2000**, *122*, 2850−2859.

(14) Yasutomi, S.; Morita, T.; Imanishi, Y.; Kimura, S. *Science* **2004**, *304*, 1944−1947.

(15) (a) Yanagisawa, K.; Morita, T.; Kimura, S. *J. Am. Chem. Soc.* **2004**, *126*, 12780−12781. (b) Miura, Y.; Kimura, S.; Kobayashi, S.; Imanishi, Y.; Umemura, J. *Biopolymer* **2000**, *55*, 391−398.

(16) (a) Xiao, X.; Xu, B.; Tao, N. *J. Am. Chem. Soc.* **2004**, *126*, 5370−5371. (b) Xiao, X.; Xu, B.; Tao, N. *Angew. Chem., Int. Ed.* **2004**, *43*, 6148−6152.

(17) Kitagawa, K.; Morita, T.; Kimura, S. *J. Phys. Chem. B* **2004**, *108*, 15090−15095.

(18) Miura, Y.; Kimura, S.; Imanishi, Y.; Umemura, J. *Langmuir* **1998**, *14*, 6935−6940.

(19) Tsuboi, M. *J. Polym. Sci.* **1962**, *59*, 139−153.

(20) Frisch, M. J.; Trucks, G. W.; Schlegel, H. B.; Scuseria, G. E.; Robb, M. A.; Cheeseman, J. R.; Montgomery, J. A., Jr.; Vreven, T.; Kudin, K. N.; Burant, J. C.; Millam, J. M.; Iyengar, S. S.; Tomasi, J.; Barone, V.; Mennucci, B.; Cossi, M.; Scalmani, G.; Rega, N.; Petersson, G. A.; Nakatsuji, H.; Hada, M.; Ehara, M.; Toyota, K.; Fukuda, R.; Hasegawa, J.; Ishida, M.; Nakajima, T.; Honda, Y.; Kitao, O.; Nakai, H.; Klene, M.; Li, X.; Knox, J. E.; Hratchian, H. P.; Cross, J. B.; Adamo, C.; Jaramillo, J.; Gomperts, R.; Stratmann, R. E.; Yazyev, O.; Austin, A. J.; Cammi, R.; Pomelli, C.; Ochterski, J. W.; Ayala, P. Y.; Morokuma, K.; Voth, G. A.; Salvador, P.; Dannenberg, J. J.; Zakrzewski, V. G.; Dapprich, S.; Daniels, A. D.; Strain, M. C.; Farkas, O.; Malick, D. K.; Rabuck, A. D.; Raghavachari, K.; Foresman, J. B.; Ortiz, J. V.; Cui, Q.; Baboul, A. G.; Clifford, S.; Cioslowski, J.; Stefanov, B. B.; Liu, G.; Liashenko, A.; Piskorz, P.; Komaromi, I.; Martin, R. L.; Fox, D. J.; Keith, T.; Al-Laham, M. A.; Peng, C. Y.; Nanayakkara, A.; Challacombe, M.; Gill, P. M. W.; Johnson, B.; Chen, W.; Wong, M. W.; Gonzalez, C.; Pople, J. A. *Gaussian 03*; Gaussian, Inc.: Pittsburgh, PA, 2004.

(21) Zhan, C.-G.; Nichols, J. A.; Dixon, D. A. *J. Phys. Chem. A* **2003**, *107*, 4184−4195.

(22) Holzwarth, G.; Doty, P. *J. Am. Chem. Soc.* **1965**, *87*, 218−228.

(23) Chen, Y. H.; Yang, J. T.; Martinez, H. M. *Biochemistry* **1972**, *11*, 4120−4131.

(24) Kennedy, D. F.; Chrisma, M.; Chapman, T. D. *Biochemistry* **1991**, *30*, 6541−6548.

(25) Poirier, G. E. *Chem. Rev.* **1997**, *97*, 1117−1127.

(26) Mayor, M.; Weber, H. B. *Angew. Chem., Int. Ed.* **2004**, *43*, 2882−2884.

(27) (a) Smit, R. H. M.; Noat, Y.; Untiedt, C.; Lang, N. D.; van Hemert, M. C.; van Ruitenbeek, J. M. *Science* **2002**, *419*, 906−909. (b) Cui, X. D.; Primak, A.; Zarate, X.; Tomfohr, J.; Sankey, O. F.; Moore, A. L.; Moore, T. A.; Gust, D.; Harris, G.; Lindsay, S. M. *Science* **2001**, *294*, 571−574. (c) Xu, B.; Tao, N. J. *Science* **2003**, *301*, 1221−1223.

(28) Salomon, A.; Cahen, D.; Lindsay, S.; Tomfohr, J.; Engelkes, V. B.; Frisbie, C. D. *Adv. Mater.* **2003**, *15*, 1881−1890.

(29) (a) Wold, D. J.; Frisbie, C. D. *J. Am. Chem. Soc.* **2001**, *123*, 5549−5556. (b) Beebe, J. M.; Engelkes, V. B.; Miller, L. L.; Frisbie, C. D. *J. Am. Chem. Soc.* **2002**, *124*, 11268−11269. (c) Engelkes, V. B.; Beebe, J. M.; Frisbie, C. D. *J. Am. Chem. Soc.* **2004**, *126*, 14287−14296.

(30) Holmlin, R. E.; Haag, R.; Chabinyc, M. L.; Ismagilov, R. F.; Cohen, A. E.; Terfort, A.; Rampi, M. A.; Whitesides, G. M. *J. Am. Chem. Soc.* **2001**, *123*, 5075−5085.

(31) (a) Wang, W.; Lee, T.; Reed, M. A. *Phys. Rev. B* **2003**, *68*, 035416. (b) Lee, T.; Wang, W.; Klemic, J. F.; Zhang, J. J.; Su, J.; Reed, M. A. *J. Phys. Chem. B* **2004**, *108*, 8742−8750.

(32) (a) Wassel, R. A.; Credo, G. M.; Fuierer, R. R.; Feldheim, D. L.; Gorman, C. B. *J. Am. Chem. Soc.* **2004**, *126*, 295−300. (b) Gorman, C. B.; Carroll, R. L.; Fuierer, R. R. *Langmuir* **2001**, *17*, 6923−6930.

(33) Simmons, J. G. *J. Appl. Phys.* **1963**, *34*, 1793−1803.

(34) Weiss, P. S.; Bumm, L. A.; Dunbar, T. D.; Burgin, T. P.; Tour, J. M.; Allara, D. L. *Ann. N.Y. Acad. Sci.* **1998** *852*, 145−177.

(35) Sisido, M.; Hoshino, S.; Kusano, H.; Kuragaki, M.; Makino, M.; Sasaki, H.; Smith, T. A.; Ghiggino, K. P. *J. Phys. Chem. B* **2001**, *105*, 10407−10415.

(36) Zhang, L.; Bain, J. A.; Zhu, J. G.; Abelmann, L.; Onoue, T. *IEEE Trans. Magn.* **2004**, *40*, 2549−2551.

(37) Datta, S.; Tian, W.; Hong, S.; Reifenberger, R.; Henderson, J. I.; Kubiak, C. P. *Phys. Rev. Lett.* **1997**, *79*, 2530−2533.

(38) Engelkes, V. B.; Beebe, J. M.; Frisbie, C. D. *J. Am. Chem. Soc.* **2004**, *126*, 14287−14296.